

Comparison of the Electrochemical Properties of Two Structurally Different Novel bis-Schiff Bases

Martina Medvidović-Kosanović*, Tomislav Balić, Berislav Marković, Anamarija Šter

Department of Chemistry, University of Osijek, Cara Hadrijana 8/A, HR-31 000 Osijek, Croatia

*E-mail: mmkosano@kemija.unios.hr

Received: 7 October 2014 / Accepted: 3 November 2014 / Published: 17 November 2014

Two novel symmetrical bis-Schiff bases ((1E)-1-N-{{4-(4-{{(E)-N-(2-aminophenyl) carboxyimidoyl} phenoxy} butoxy) phenyl}methylidene}benzene-1,2-diamine (compound 1) and (1E)-1-N-{{4-(4-{{(E)-N-(4-aminophenyl) carboxyimidoyl} phenoxy} butoxy) phenyl}methylidene}benzene-1,4-diamine (compound 2) were synthesized and characterized by means of single-crystal X-ray diffraction (1), FT-IR and NMR spectroscopy (1,2), elemental (1,2), TG/DSC and electrochemical analysis (1,2). The prepared compounds are positional isomers that display very different electrochemical behaviour. Electrochemical study has shown that the oxidation of the investigated Schiff base (1) is irreversible, diffusion controlled process, and that the oxidation products are adsorbed on the glassy carbon electrode surface. Oxidation of a Schiff base (2) is reversible (follows EC reaction mechanism), diffusion controlled, and the oxidation products are also adsorbed on the glassy carbon electrode surface. Considering molecular structure of compounds, molecule 1 is planar, with small deviation of atoms from the calculated plane. The planarity of molecule 1 is stabilized by untypical intramolecular interaction of amino and imino nitrogen atoms. In the crystal, the molecules are primarily linked by hydrogen bonds involving primary amino groups and weak C-H \cdots π interactions. Consequently, these interactions are arranging molecules into herringbone packing motif. Crystal structure of molecule 2 could not be determined but it is predicted based upon similarity with molecule 1 and interpretation of the spectral data (NMR and FTIR).

Keywords: voltammetry, structure related electrochemical properties, bis-Schiff base, single-crystal X-ray analysis, NMR, IR, TG/DSC

1. INTRODUCTION

Recently, symmetrical bis-Schiff bases were used in the design of liquid crystal materials [1], as the building blocks for the synthesis of liquid crystal polymers or oligomers [2] and for preparation of the organic thin-film transistors [3]. Schiff bases are also widely studied due to their biological and

pharmacological activity [4], optical [5], photochromical [6], thermochromical [7] properties and other outstanding properties. Among other factors, above mentioned properties (including electrochemical) of symmetrical bis-Schiff bases depend on a molecular structure of a compound and crystal packing of the molecules [8].

Untill now, Schiff bases and their metal complexes have been studied by XRD [9], EDX [9], TGA/DTA [9], SEM [9], TEM [9], FT-IR spectroscopy [9-14], ^1H NMR [10, 11, 15], fluorescence [11], EPR [12], conductometry [11, 14], elemental analysis [11-14] and UV/Vis spectroscopy [14, 15]. Their structure was determined by ab initio calculations [12] and X-ray diffraction [10-14], and electrochemical characterization was conducted by square wave voltammetry [15] and cyclic voltammetry [11, 13, 14, 16-18]. Biological activity and possible use of Schiff bases as potentiometric sensors for metal cation determination was also studied [19-23].

In this study we have synthesized two molecules that are rare examples of a symmetrical bis-Schiff base with uncondensed primary amino group (with few known examples of similar structures [24,25]). The compounds were characterized by means of single crystal X-ray diffraction, IR spectroscopy, NMR spectroscopy, TG/DSC analysis and elemental analysis. Since electrochemical techniques are widely used for the analysis of molecules with electrochemical activity due to the advantages of rapid response, low cost, high sensitivity, and real-time detection, we have used voltammetric techniques (cyclic and differential pulse voltammetry) to study electrochemical properties of Schiff bases. In this study we report different oxido reduction properties of two novel symmetrical bis-Schiff bases (Scheme 1) caused by the differences in their molecular structure.

2. EXPERIMENTAL

2.1 Chemicals and apparatus

All commercially available chemicals were of reagent grade and used as purchased. Dialdehyde 4-[4-(4-formylphenoxy)butoxy]benzaldehyde was prepared by previously reported method [26]. N, N-dimethylformamide (DMF) was purchased from Fischer Chemical and lithium chloride (LiCl) from BDH Prolabo and were used without further purification.

IR spectra were recorded on a Shimadzu FTIR 8400S spectrophotometer using the DRS 8000 attachment, in the $4000\text{-}400\text{ cm}^{-1}$ region. Thermogravimetric analysis was performed using a simultaneous TGA-DSC analyser (Mettler-Toledo TGA/DSC 1). The compounds were placed in aluminium pan (100 μL) and heated in nitrogen atmosphere (200 mL min^{-1}) up to $590\text{ }^\circ\text{C}$ at a rate of $10\text{ }^\circ\text{C min}^{-1}$. The data collection and analysis was performed using the program package STAR^e Software 10.0 [27]. C, H, N analyses were provided by the Analytical Services Laboratory of the Ruđer Bošković Institute, Zagreb. The ^1H NMR and ^{13}C NMR were recorded on NMR (300 MHz) Bruker instrument, using deuterated chloroform and DMSO as solvents at NMR Laboratory of the Ruđer Bošković Institute, Zagreb.

The X-ray diffraction data of compound 1 were collected at room temperature on an Oxford Diffraction Xcalibur 3 CCD diffractometer with graphite-monochromated Mo- K_α radiation ($\lambda =$

0.71073 Å) using ω -scans. The data reduction was performed using the CrysAlis software package [28]. The structure was solved using SIR2004 [29]. Refinement and analysis of the structure were done by using the programs integrated in the WinGX system [30]. The refinement procedure was performed using SHELXL-97 [31]. The non-hydrogen atoms were refined anisotropically. Hydrogen atoms in the structure were placed in calculated positions and refined using the riding model except amino hydrogen atoms that were located in differential Fourier map and refined freely. Geometrical calculations were done using PLATON [32, 33] and the structure drawings with ORTEP - III [34].

Electrochemical experiments were performed on PalmSens potentiostat/galvanostat (PalmSens BV, Utrecht, The Netherlands) driven by PSTrace 4.2 software. A conventional three-electrode cell was used with a glassy carbon as a working electrode, non-aqueous Ag/Ag⁺ as a reference electrode and a platinum wire as a counter electrode. The glassy carbon working electrode was polished with coarse diamond polish (1 μm , ALS, Japan) and with polishing α -Al₂O₃ (0.05 μm , ALS, Japan) before each measurement. Cyclic voltammetry scan rate was 100 mV s⁻¹, and the differential pulse voltammetry conditions were: scan increment 5 mV, pulse amplitude 25 mV, pulse width 70 ms, and scan rate 5 mV s⁻¹.

2.2. Synthesis of compounds

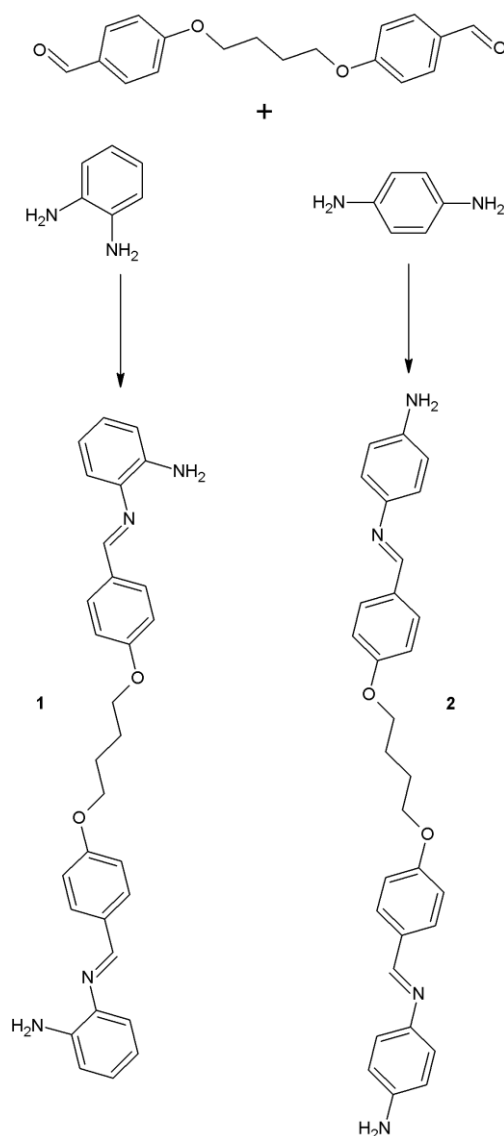
The compounds were synthesized according to Scheme 1. Dialdehyde, as a starting material, was prepared according to previously reported method [26], as following: 50 mmol of p-hydroxybenzaldehyde and 50 mmol of K₂CO₃ were mixed in DMF and the mixture was brought to the reflux temperature. 25 mmol of butane-1,4-dibrom dissolved in 5 ml of DMF was gradually added to the reaction mixture and the reaction was carried out for 5 h. When the reaction was completed, 100 ml of deionized water was added and precipitate was filtered and washed with water. Resulting yellow crystalline product was recrystallized from ethanol/water mixture. Yield: 55 %, melting point (DSC): 108 °C. Significant IR data: 2954 cm⁻¹ and 2876 cm⁻¹ (C–H stretching), 1675 cm⁻¹ (C=O stretching), 1244 cm⁻¹ (C–O–C stretching).

2.2.1. Synthesis of Schiff base (1E)-1-N-[[4-(4-[(E)-N-(2-aminophenyl) carboxyimidoyl] phenoxy) butoxy) phenyl]methylidene}benzene-1,2-diamine (compound 1)

Dialdehyde (0.6 g, 2 mmol) was dissolved in 40 ml of methanol and 2-3 drops of glacial acetic acid were added to this solution. The solution was brought to brisk reflux and 0.49 g (4.5 mmol) of o-phenylenediamine dissolved in 25 ml of methanol was gradually added. The mixture was heated at reflux temperature ($\theta = 65$ °C) for 3 hours. After the reaction was completed, the resulting mixture was left at room temperature ($\theta = 25$ °C) for 24 hours. The yellow crystalline product was filtered and washed with cold ethanol and diethyl ether. The product was recrystallized from benzene to yield pure product as yellow crystals. Single crystals suitable for X-ray diffraction experiments were obtained by slow evaporation of benzene solution. Yield: 82%. M. p. (DSC): 163 °C. Anal. Calc. for C₃₀ H₃₀N₄O₂: C, 75.29; H, 6.32; N, 11.71. Found: C, 74.44; H, 6.58; N, 9.98%.

2.2.2. Synthesis of Schiff base (1E)-1-N-[[4-(4-[[[(E)-N-(4-aminophenyl) carboxyimidoyl] phenoxy] butoxy) phenyl] methylidene} benzene-1,4-diamine (compound 2)

Dialdehyde (0.6 g, 2 mmol) was dissolved in 40 ml of methanol and 2-3 drops of glacial acetic acid were added. The solution was brought to brisk reflux and 0.49 g (4.5 mmol) of p-phenylenediamine dissolved in 25 ml of methanol was gradually added. The mixture was heated at reflux temperature for 3 hours. After the reaction was completed, the resulting mixture was left at room temperature for 24 hours. The red powder product was filtered and washed with cold ethanol and diethyl ether. Yield: 76 % M. p. (DSC): 442 °C (thermal decomposition). Anal. Calc. for $C_{30}H_{30}N_4O_2$: C, 75.29; H, 6.32, N; 11.71. Found: C, 75.53; H, 6.22; N, 8.70%.



Scheme 1. Synthetic pathway for synthesis of compounds 1 and 2

3. RESULTS AND DISCUSSION

Prepared compounds are positional isomers regarding the position of primary amino group. These compounds, as frequently is the case, show different properties. For example, compound 1 is readily soluble in most common organic solvents, while 2 is insoluble in many common solvents (some solubility is observed in polar organic solvents such as DMSO and DMF). Also, as it will be discussed later, there are significant differences in thermal stability and electrochemical behavior of these compounds. The abovementioned properties are most probably the consequence of packing arrangement of molecules and molecular forces acting between them in the solid state. Unfortunately, all efforts considering the preparation of crystals suitable for a single-crystal X-ray diffraction failed in the case of compound 2. However, the crystal structure of compound 1 is determined and due to the similarity of the prepared compounds (and in the correlation with the spectral studies) we can almost certainly determine molecular structure of compound 2 (depicted in Scheme 1.).

3.1. Spectral and thermal characterization of compounds

The IR spectra of compounds 1 and 2 are represented in Figure 1. The IR spectra of both compounds exhibit bands due to $\nu(\text{N-H})$ stretching vibration of the primary amino group at 3450 cm^{-1} and 3360 cm^{-1} for compound 1 and 3558 cm^{-1} and 3383 cm^{-1} for compound 2. Small differences in stretching vibrations of primary amino group of compounds are caused by the presence of strong intramolecular interaction in compound 1. The vibrations close to 2950 cm^{-1} and 2870 cm^{-1} are due to aliphatic C-H stretching. The C=N stretching vibration of compound 1 is coupled with C-C stretching vibration of aromatic ring and is located around 1600 cm^{-1} . For compound 2 azomethine stretching vibration appears at 1619 cm^{-1} . Also, the spectra of both compounds exhibit strong vibration at 1248 cm^{-1} that is assigned to stretching of $\text{C}_{\text{aromatic}}\text{-O-C}_{\text{aliphatic}}$ group. The most pronounced differences in IR spectra of compounds are in the area from 850 cm^{-1} up to 750 cm^{-1} (out-of-plane C-H bending vibrations of benzene rings). For compound 1 these vibrations appear at 836 cm^{-1} and 743 cm^{-1} and are assigned to C-H bending vibrations of para and ortho substituted benzene ring, respectively. For compound 2 vibration at 849 cm^{-1} is assigned to C-H bending vibration of para substituted benzene ring.

In the ^1H NMR spectra of compounds there are multiplet signals at 6.6–7.9 ppm corresponding to aromatic protons. Methylene protons signal of aliphatic chain occurs in the region between 1.90 ppm and 4.2 ppm. The imine protons signal for both compounds appears at 8.47 ppm. Most pronounced difference in the spectra is in the chemical shifts of primary amine protons 5.34 and 4.96 ppm for compounds 1 and 2, respectively. The ^{13}C NMR spectrum exhibits signals at 25.94 ppm and 67.62 ppm for compound 1, 25.87 ppm and 67.99 ppm for compound 2 corresponding to the methylene carbons. The aromatic carbons chemical shifts signals are located in the interval from 114.6 ppm up to 157.0 ppm for compounds 1 and 2. The carbon atom of the imine group exhibits chemical shift at 161.48 ppm and 161.05 ppm for 1 and 2, respectively.

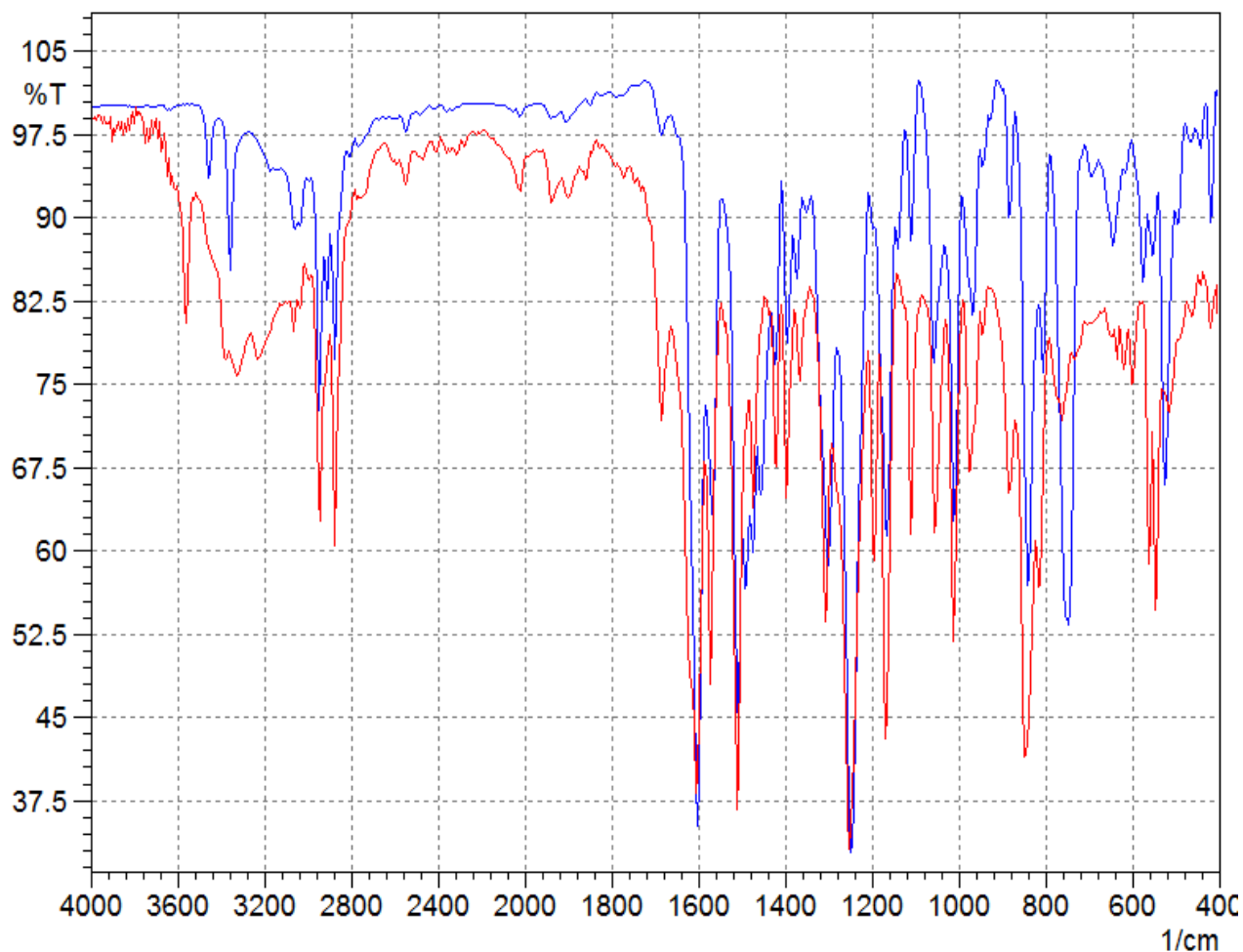


Figure 1. IR spectra of compound 1 (blue line) and compound 2 (red line).

The TG and DSC curves of the compounds are represented in Figure 2. TG curve of compound 1 shows two-step thermal decomposition. The first thermal event starts at 173 °C with experimental mass loss of 7.6 % and could be related to thermal decomposition of primary amino groups (calc. 6.7 %). The second thermal event is at 387 °C and can be related to the thermal decomposition of compound 1. The DSC curve exhibits only one endothermic event at 165 °C that is related to the melting point of compound 1. The TG curve of compound 2 also exhibits two-step thermal decomposition. Similar to the compound 1, the first thermal event can be attributed to the decomposition of primary amino groups in compound 2. The second thermal event is also attributed to thermal decomposition of compound 2. The DSC curve does not exhibit any thermal events that could be related to the melting point of compound 2 or some other phase transition events. Considering temperature of the thermal decomposition of compounds, it can be noticed that compound 1 shows higher thermal stability, most probably due to stronger molecular interactions in the solid state.

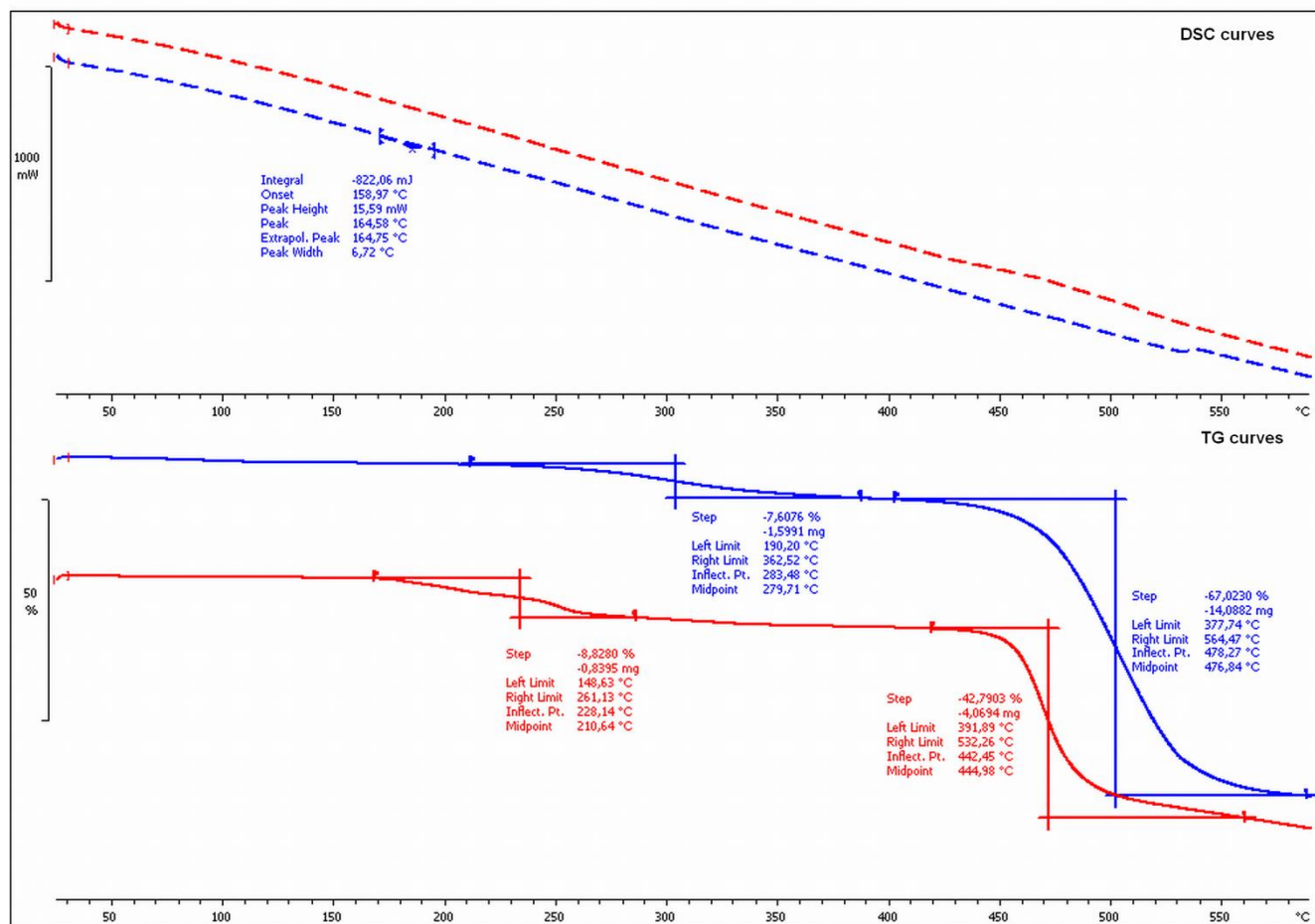


Figure 2. TG and DSC curves of compound 1 (blue lines) and compound 2 (red lines).

3.2. Crystal structure of compound 1

The crystallographic data and structure refinement details are given in Table 1. The molecule crystallizes in orthorhombic system with space group *P bca*. The asymmetric unit of the compound comprises only one half of the molecule with crystallographic inversion centre lying in the centre of the molecule. ORTEP plot of the crystal structure is represented by Fig. 3. Bond distances and angles are within the normal ranges and are in close agreement with literature values [35].

The molecule is essentially planar, with largest out-of-plane deviation $4.93(1)^\circ$ of aminophenyl benzene ring from the plane calculated through the aliphatic chain. The largest deviation of a single atoms from the least-squares plane are $0.1518(1) \text{ \AA}$ and $0.129(2) \text{ \AA}$ of the imino and amino nitrogen atoms, respectively. The aliphatic chain is in all *trans* conformation, which consequently contributes to planarity of the molecule. The molecule adopts (*E*) - conformation about imine N2–C7 bond with the torsion angle C8–C7–N2–C6 of $-179.5(2)^\circ$.

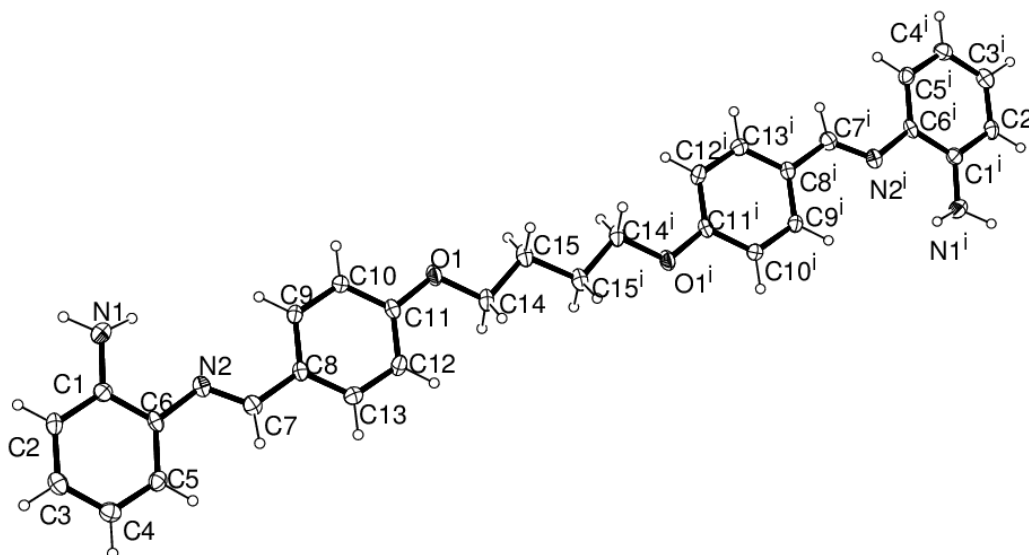


Figure 3. ORTEP plot of structure of compound 1 with displacement ellipsoids of non-hydrogen atoms drawn at 50% probability level.

Table 1. Crystallographic data and structure refinement details for compound 1.

| | |
|---|---|
| Empirical formula | C ₃₀ H ₃₀ N ₄ O ₂ |
| <i>M_r</i> | 478.58 |
| <i>T</i> (K) | 294(2) |
| crystal colour, habit | yellow plate |
| crystal size (mm ³) | 0.52 × 0.35 × 0.06 |
| crystal system | orthorhombic |
| space group | <i>P bca</i> |
| unit cell parameters | |
| <i>a</i> (Å) | 10.1933(9) |
| <i>b</i> (Å) | 6.8890(6) |
| <i>c</i> (Å) | 35.214(3) |
| <i>V</i> (Å ³) | 2472.8(4) |
| <i>Z</i> | 4 |
| <i>D</i> _{calc} (g cm ⁻³) | 1.286 |
| <i>μ</i> (mm ⁻¹) | 0.082 |
| <i>F</i> (000) | 1016 |
| total data | 8674 |
| number of unique data | 2425 |
| number of parameters | 171 |
| <i>R</i> ₁ ^a , [<i>F</i> _o ≥ 4σ(<i>F</i> _o)] | 0.0577 |
| <i>wR</i> ₂ ^b | 0.1044 |
| Goodness of fit on <i>F</i> ² , <i>S</i> | 1.012 |
| Min. and max. electron density (e Å ⁻³) | 0.272, -0.175 |

$$^a R = \frac{\sum ||F_o| - |F_c||}{\sum |F_o|}$$

$$^b wR = [\sum (F_o^2 - F_c^2)^2 / \sum w(F_o^2)^2]^{1/2}$$

The strong intramolecular hydrogen bond N1–H101⋯N2 (2.698(3) Å) subsequently contributes to planarity of the molecule. Considering intermolecular interactions, it can be observed that the molecules are arranged in a herringbone packing motif. This type of packing arrangement is typical for long planar molecules [1-3]. List of the selected bond lengths, bond and torsion angles are given in Table 2. Hydrogen bonds geometry is given in Table 3.

Table 2. Selected interatomic bond distances (Å), bond angles (°) and torsion angles (°) for compound 1.

| Selected bond distances (Å) | | Selected bond angles (°) | | Selected torsion angles (°) | |
|-----------------------------|----------|--------------------------|-----------|-----------------------------|------------|
| C1-N1 | 1.373(3) | N2-C7-C8 | 123.0(2) | N1-C1-C6-N2 | -3.4(3) |
| C6-N2 | 1.421(3) | O1-C14-C15 | 108.03(1) | O1-C14-C15-C15# | -177.6(2) |
| C7-N2 | 1.268(3) | C14-C15-C15# | 110.9(3) | C15-C14-O1-C11 | -178.62(1) |
| C11-O1 | 1.367(3) | C11-O1-C14 | 117.56(1) | C8-C7-N2-C6 | -179.5(2) |
| C14-O1 | 1.428(3) | C7-N2-C6 | 120.7(2) | | |

#-x+1,-y,-z+1

Table 3. Hydrogen bond geometry (Å, °) for compound 1.

| D–H⋯A | <i>d</i> (D–H) | <i>d</i> (H⋯A) | <i>d</i> (D⋯A) | ∠(DHA) | Symmetry code |
|---------------|----------------|-----------------|-----------------|---------|-------------------------|
| C9-H9⋯N1 | 0.95 | 2.84 | 3.268(3) | 108.2 | -x + 1, -y, -z + 1 |
| N1-H100⋯N2 | 0.95 | 2.52 | 3.312(3) | 141 | -x + 1/2, y + 1/2, z |
| N1-H101⋯N1 | 0.994 | 2.279 | 2.698(3) | 104 | x, y, z |
| D–H⋯A | <i>d</i> (D–H) | <i>d</i> (H⋯Cg) | <i>d</i> (D⋯Cg) | ∠(DHCg) | Symmetry code |
| C(3)-H(3)⋯Cg1 | 0.95 | 2.75 | 3.6(3) | 149 | 1 - x, 1/2 + y, 1/2 - z |
| C15-H15B⋯Cg2 | 0.99 | 2.88 | 3.775(3) | 152 | 1 - x, 1 - y, 1 - z |

3.3. Interpretation of molecular structure of compound 2

The prepared compounds are positional isomers regarding the position of primary amino group. Primary amino group is in ortho and para position in 1 and 2, respectively. If we compare spectral data of the prepared compounds it can be deduced: (i) FTIR spectra (Fig. 2.) of both compounds exhibit vibrations characteristic for the mutual dialdehyde precursor. Furthermore, both spectra exhibit vibrations characteristic for the primary amino group. Both spectra are free of the vibrations typical for a carbonyl group; (ii) NMR spectra of both compounds exhibit chemical shifts characteristic for common dialdehyde precursor and primary amino group and are free of a carbonyl group chemical shifts; (iii) Thermal studies of both compounds display two-step thermal decomposition, most probably with the identical decomposition mechanism. These results indicate that the molecular structure of 2 is very similar to the molecular structure of 1. The molecule 2 is most probably symmetrical, with inversion centre in the middle of aliphatic chain (C_i symmetry), planar and with similar conformation

characteristics as in 1. As previously mentioned, there are some differences in the position of primary amino group vibrations, both in NMR and FTIR spectra. Therefore, it is reasonable to assume that inter/intra molecular interactions are substantially different in 1 and 2 and are the reason for different electrochemical behaviour.

3.4. Cyclic voltammetry studies

A cyclic voltammogram of the investigated compound 1 is shown in Fig. 4. Only one anodic peak (A1) is visible at a potential of 0.677 V when the potential was scanned from -0.6 V to 1.0 V vs. Ag/Ag⁺ reference electrode. The oxidation reaction involves the transfer of one electron which probably leads to formation of a radical cation [36]. No reduction wave can be observed, indicating that the oxidation reaction is totally irreversible.

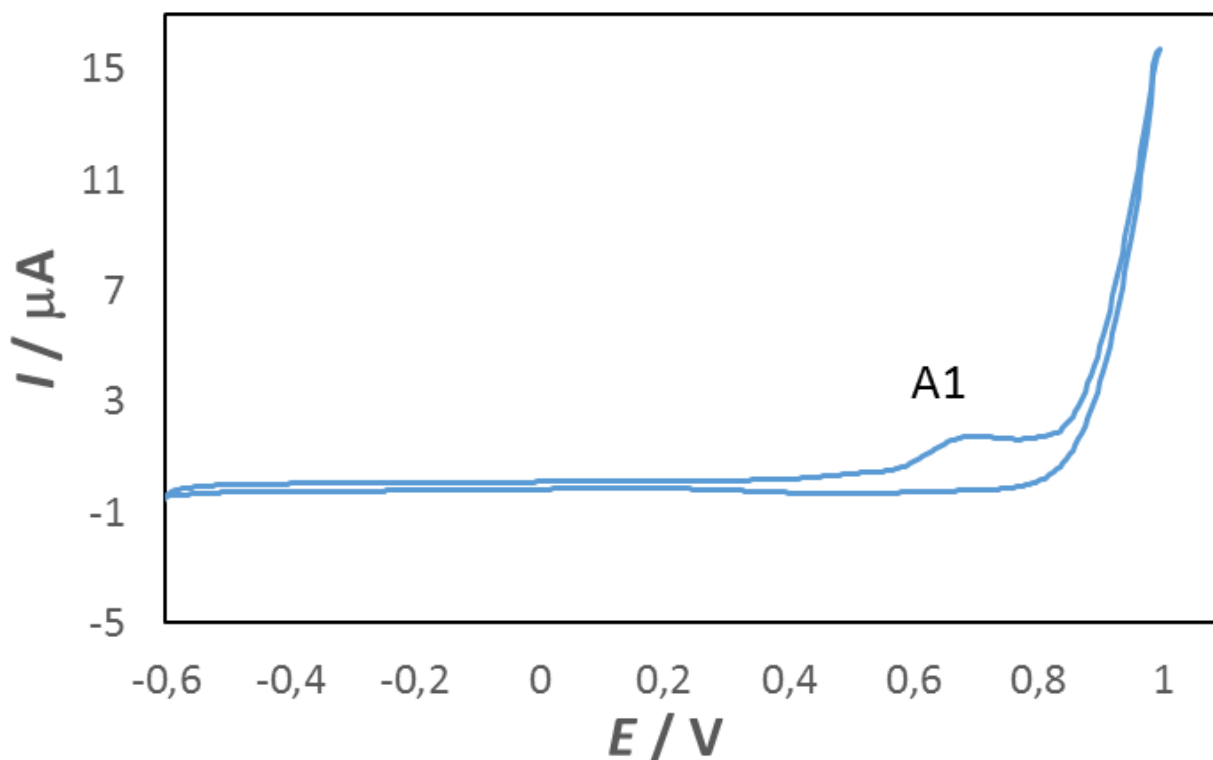


Figure 4. Cyclic voltammogram of compound 1 ($c = 5.9 \cdot 10^{-4} \text{ mol dm}^{-3}$) at a glassy carbon electrode ($I_c = 0.1 \text{ M LiCl}$ in DMF). Scan rate: 100 mV/s.

A cyclic voltammogram of the investigated compound 2 is shown in Fig. 5. One anodic (A1) peak at a potential of 0.456 V and one cathodic (K1) peak at a potential 0.396 V appeared when the potential was scanned from -0.2 V to 0.8 V vs. Ag/Ag⁺ reference electrode. Obtained ΔE_p value is 60 mV, which indicates that the oxidation reaction is reversible. Possible mechanism of the oxidation process could involve the following steps: first step includes transfer of one electron which leads to

formation of a radical cation, then follows the second step which includes deprotonation and formation of an amine radical which binds to a glassy carbon electrode surface [36]. Reduction process includes reduction of an amine radical to an amine.

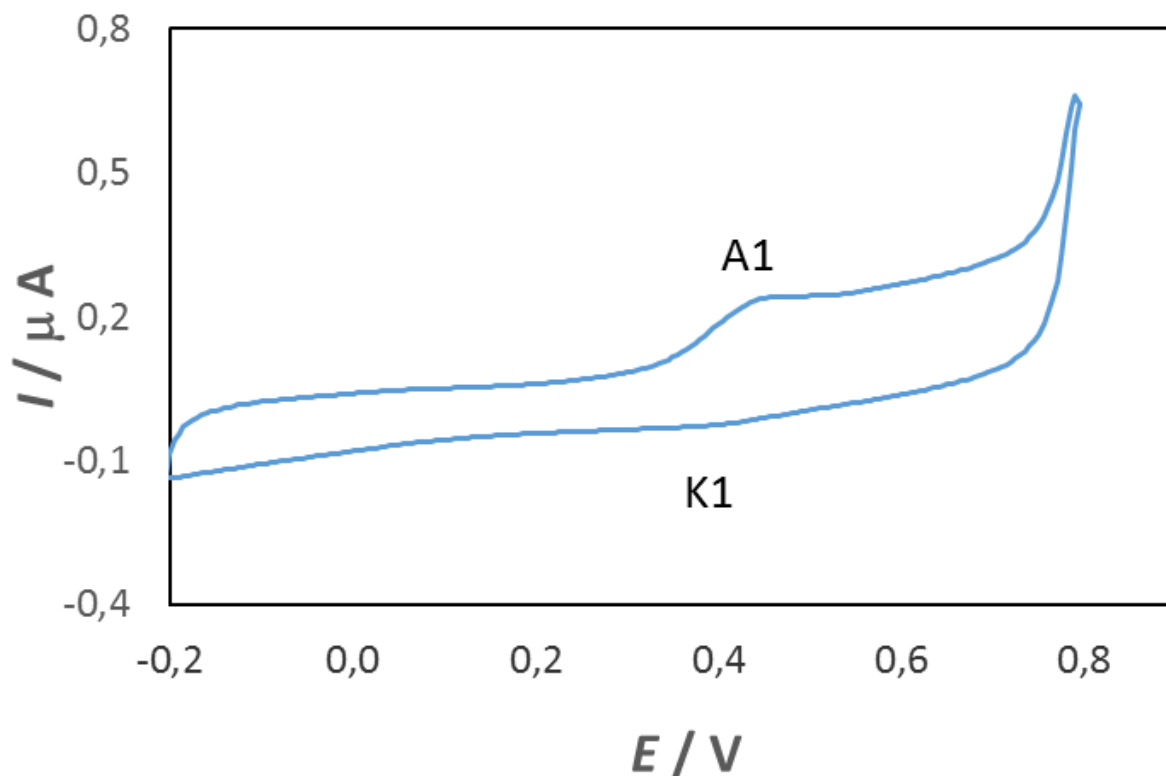


Figure 5. Cyclic voltammogram of compound 2 ($c = 1.1 \cdot 10^{-4} \text{ mol dm}^{-3}$) at a glassy carbon electrode ($I_c = 0.1 \text{ M LiCl}$ in DMF). Scan rate: 100 mV/s.

The influence of concentration of the investigated Schiff bases on anodic peak current and anodic peak potential was examined (data obtained for compound 1 are given in Table 4). The effect of scan rate on the oxidation of the Schiff bases has been investigated as well (Fig. 6). It was observed that both anodic peak potential and anodic peak current increase with the increase in Schiff bases concentration and scan rate. The cathodic peak current of compound 2 also increases with scan rate and the ΔE_p is around 60 mV (it increases significantly at higher scan rates). Cathodic peak potential decreases toward more negative potential values and $I_{p,c} / \nu^{1/2}$ ratio is around $3.3 \cdot 10^{-6} \text{ C V}^{-1}$ with increasing scan rate (Table 5) which agrees with EC reaction mechanism (reversible electrode reaction followed by reversible chemical reaction) [37].

Table 4. Anodic peak potential ($E_{p,a}$) and anodic peak current ($I_{p,a}$) of compound 1 as the function of its concentration. Scan rate: 100 mV/s.

| $10^4 \cdot c / \text{mol dm}^{-3}$ | $E_{p,a} / \text{V}$ | $I_{p,a} / \mu\text{A}$ |
|-------------------------------------|----------------------|-------------------------|
| 0.5 | 0.579 | 0.532 |
| 1.9 | 0.599 | 0.696 |
| 2.8 | 0.618 | 1.304 |
| 4.5 | 0.646 | 1.848 |
| 5.4 | 0.679 | 2.120 |
| 6.1 | 0.689 | 2.337 |

Table 5. Cathodic peak potential ($E_{p,c}$), cathodic peak current ($I_{p,c}$), ΔE_p and $(I_{p,c} / \nu^{1/2})$ ratio of compound 2 as the function of a scan rate.

| $\nu / \text{mV s}^{-1}$ | $E_{p,c} / \text{V}$ | $10^2 I_{p,c} / \mu\text{A}$ | $\Delta E_p / \text{mV}$ | $10^6 (I_{p,c} / \nu^{1/2}) / \text{CV}^{-1}$ |
|--------------------------|----------------------|------------------------------|--------------------------|---|
| 75 | 0.4025 | 1.652 | 54 | 1.9 |
| 100 | 0.396 | 2.826 | 60 | 2.8 |
| 150 | 0.393 | 3.783 | 66 | 3.1 |
| 200 | 0.393 | 5.304 | 66 | 3.8 |
| 250 | 0.387 | 6.217 | 91 | 3.9 |
| 300 | 0.387 | 7.130 | 95 | 4.1 |

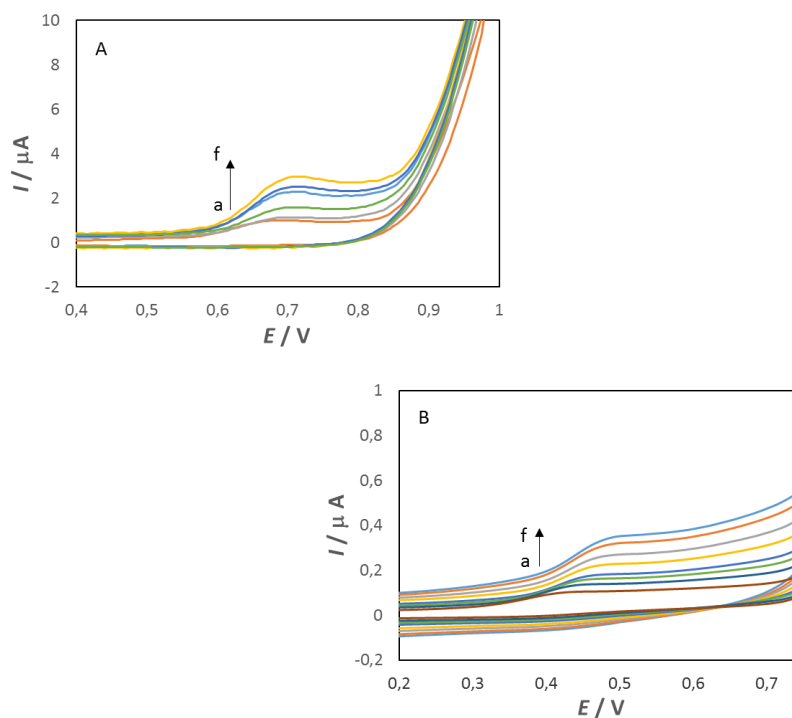
**Figure 6.** Cyclic voltammograms of compound 1 (figure 6A) and compound 2 (figure 6B) at a glassy carbon electrode ($I_c = 0.1 \text{ M LiCl}$ in DMF) at different scan rates ($\nu = 25, 75, 150, 200, 250$ and 300 mV/s (curves a-f)).

Fig. 7 shows that at lower concentrations of compound 1 (below $c \sim 1.3 \cdot 10^{-4} \text{ mol dm}^{-3}$) anodic peak current is a linear function of the Schiff base concentration, which indicates that oxidation product of the investigated Schiff base (radical cation formed in one electrode transfer reaction) is adsorbed on the glassy carbon electrode surface. At higher concentrations of compound 1 (above $c \sim 1.3 \cdot 10^{-4} \text{ mol dm}^{-3}$), the increase of peak current slows down. Similar behaviour was observed for compound 2. At lower concentrations of compound 2 (below $c \sim 1.1 \cdot 10^{-4} \text{ mol dm}^{-3}$) anodic peak current is a linear function of the Schiff base concentration (the adsorption of the investigated Schiff base oxidation product, amine radical, on the electrode surface is taking place). At higher concentrations of compound 2 (above $c \sim 1.1 \cdot 10^{-4} \text{ mol dm}^{-3}$), the increase of peak current slows down. This behavior could be explained by increase of interactions between oxidation products adsorbed on the electrode surface and by diffusion current [38, 39].

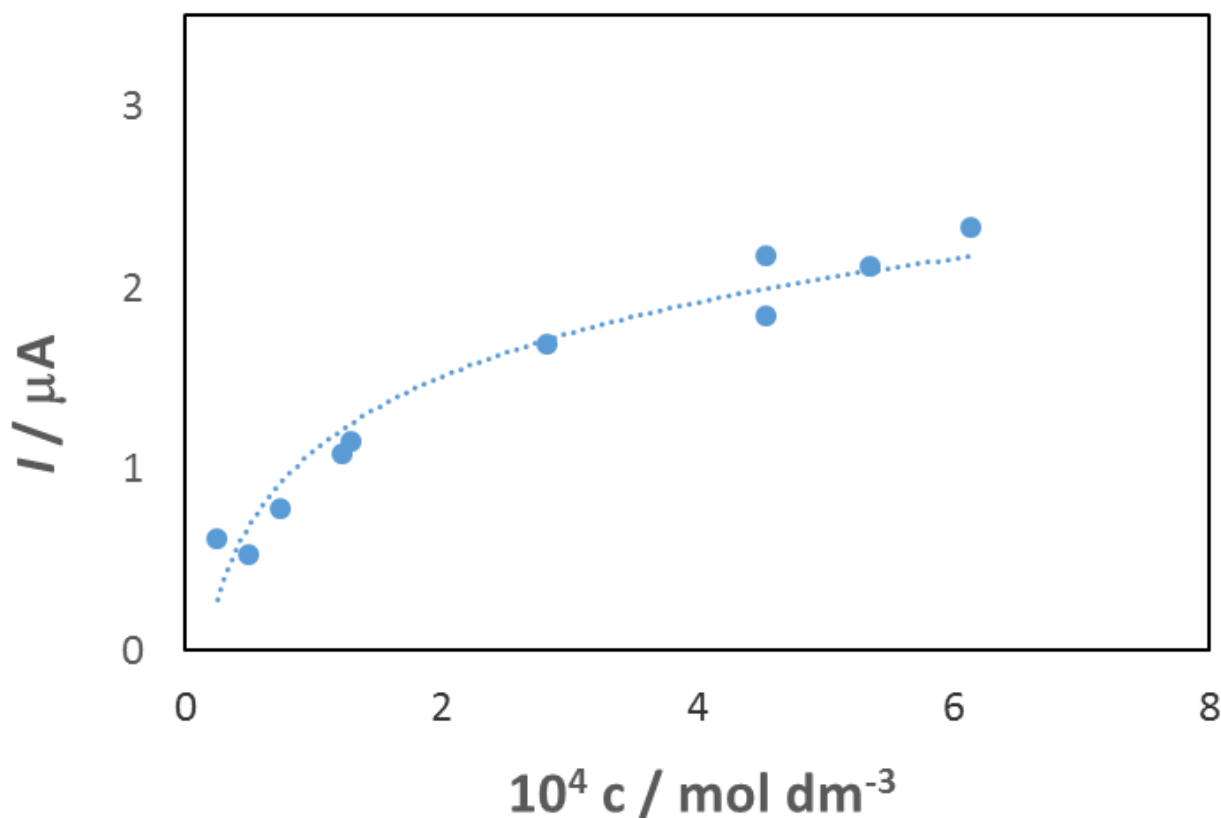


Figure 7. Anodic peak current as a function of compound 1 concentration ($I_c = 0.1 \text{ M LiCl}$ in DMF). Scan rate: 100 mV/s.

It can also be seen from Fig. 8 that the oxidation of compound 1 and 2 is diffusion controlled since linear dependence was found, for both Schiff bases, between anodic peak current and the square root of scan rate [39, 40].

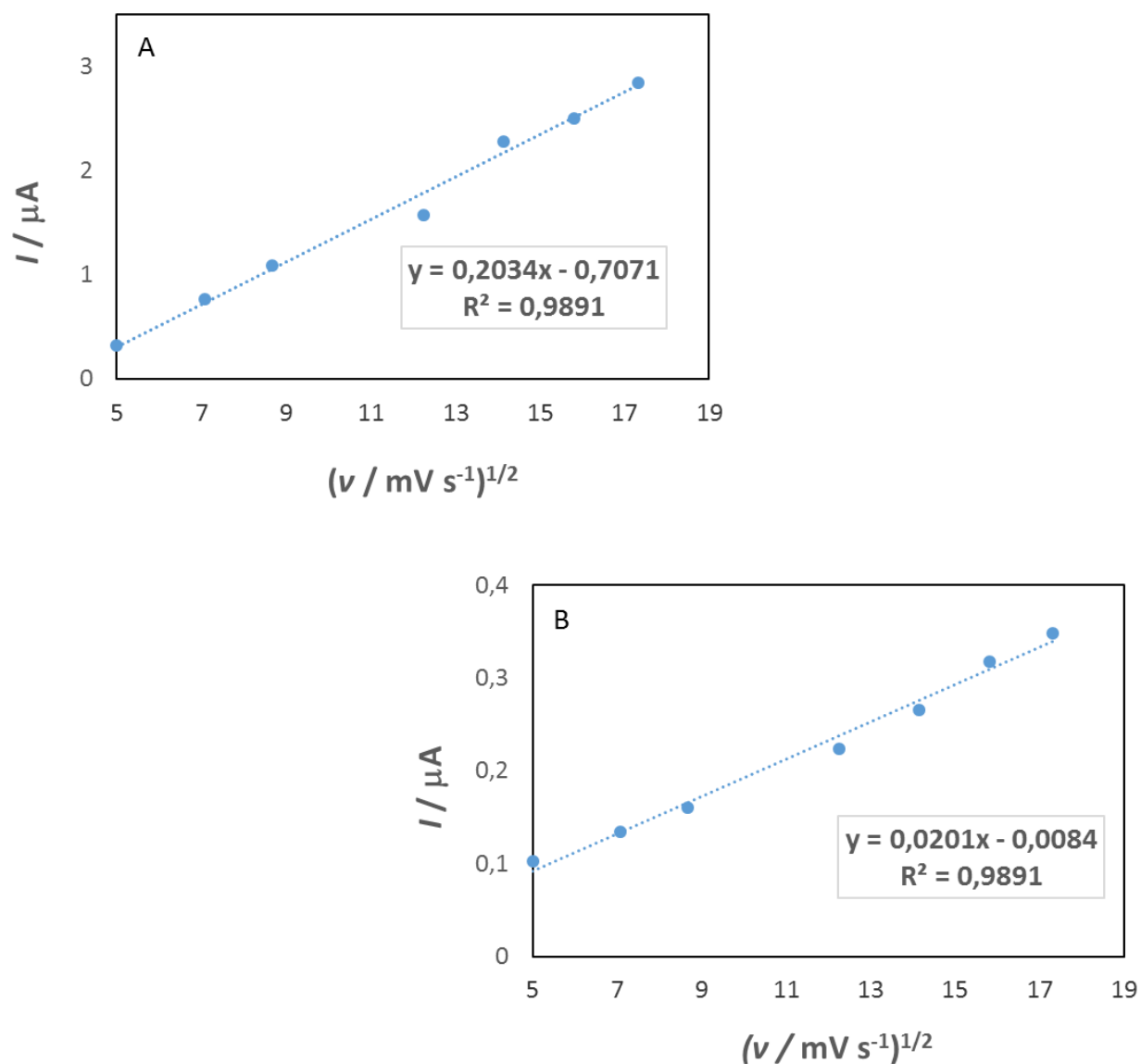


Figure 8. Anodic peak current, I , as a function of the square root of scan rate, $v^{1/2}$, at a glassy carbon electrode in solution of compound **1** (figure 8A) and compound **2** (figure 8B) ($I_c = 0.1 \text{ M LiCl}$ in DMF).

3.5. Differential pulse voltammetry studies

Differential pulse voltammogram in Fig. 9 also reveals one oxidation peak of the investigated compound **1** at the potential 0.630 V. The oxidation peak decreases with successive scans which confirms adsorption of the compound **1** oxidation products on the glassy carbon electrode surface.

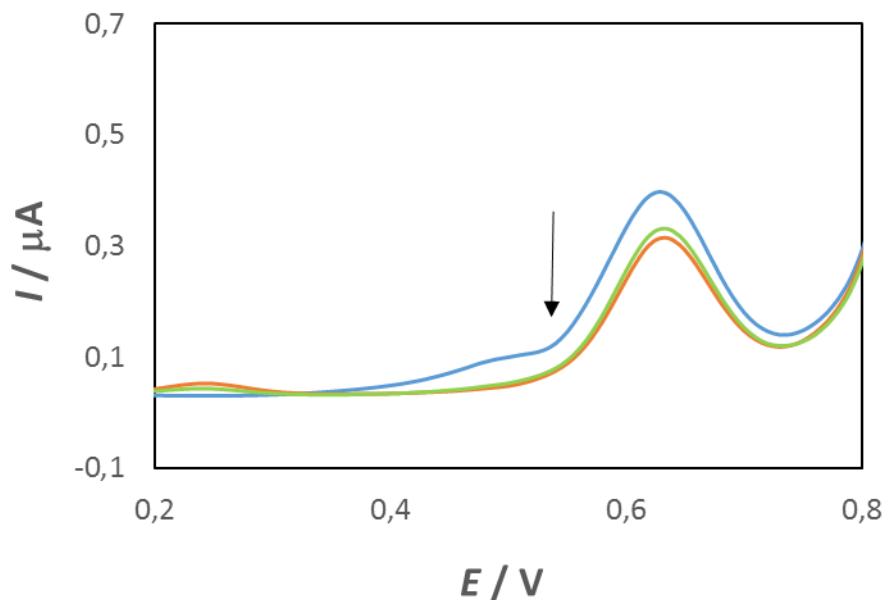


Figure 9. Differential pulse voltammogram of Schiff base (1) ($c = 5.9 \cdot 10^{-4} \text{ mol dm}^{-3}$) at a glassy carbon electrode ($I_c = 0,1 \text{ M LiCl}$ in DMF). Scan rate: 5 mV/s. First scan (—), third scan (—), fourth scan (—).

Differential pulse voltammogram in Fig. 10 reveals one oxidation peak of the investigated compound 2 at the potential 0.415 V. The oxidation peak decreases with successive scans which also confirms adsorption of the Schiff base oxidation products on the glassy carbon electrode surface.

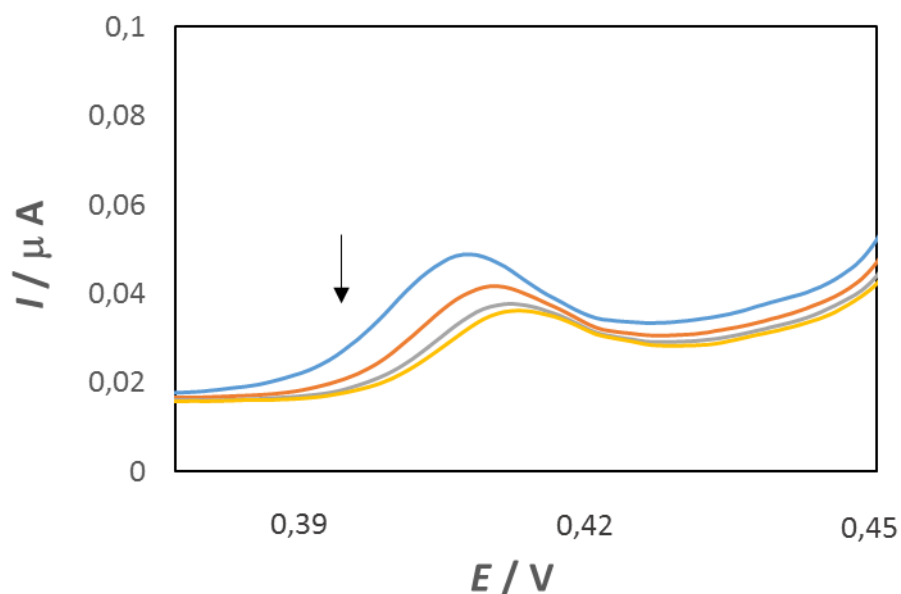


Figure 10. Differential pulse voltammogram of compound 2 ($c = 1.1 \cdot 10^{-4} \text{ mol dm}^{-3}$) at a glassy carbon electrode ($I_c = 0,1 \text{ M LiCl}$ in DMF). Scan rate: 5 mV/s. First scan (—), second scan (—), third scan (—), fourth scan (—).

Peak current and peak potential of both Schiff bases increase with increasing compound 1 and 2 concentrations, which could be explained by kinetic limitation in the reaction between the redox sites of a glassy carbon electrode and the investigated Schiff base [17]. A linear relationship could be established between peak current and compound 1 concentration in the range of $0.3 \cdot 10^{-4} \text{ mol dm}^{-3}$ to $6.10 \cdot 10^{-4} \text{ mol dm}^{-3}$ (Fig. 11). A linear regression equation, $I_p = 0.0504 c + 0.023$ with a correlation coefficient $R^2 = 0.9747$, can be obtained, where I_p is the oxidation peak current and c is the compound 1 concentration ($\cdot 10^{-4} \text{ mol dm}^{-3}$). Linear relationship between peak current and compound 2 concentration in the range of $0.3 \cdot 10^{-4} \text{ mol dm}^{-3}$ to $1.4 \cdot 10^{-4} \text{ mol dm}^{-3}$ was also established (Fig. 12). A linear regression equation, $I_p = 2.4283 c + 1.8699$ with a correlation coefficient $R^2 = 0.9663$, can be obtained, where I_p is the oxidation peak current ($\cdot 10^{-2} \mu\text{A}$) and c is the compound 2 concentration ($\cdot 10^{-4} \text{ mol dm}^{-3}$).

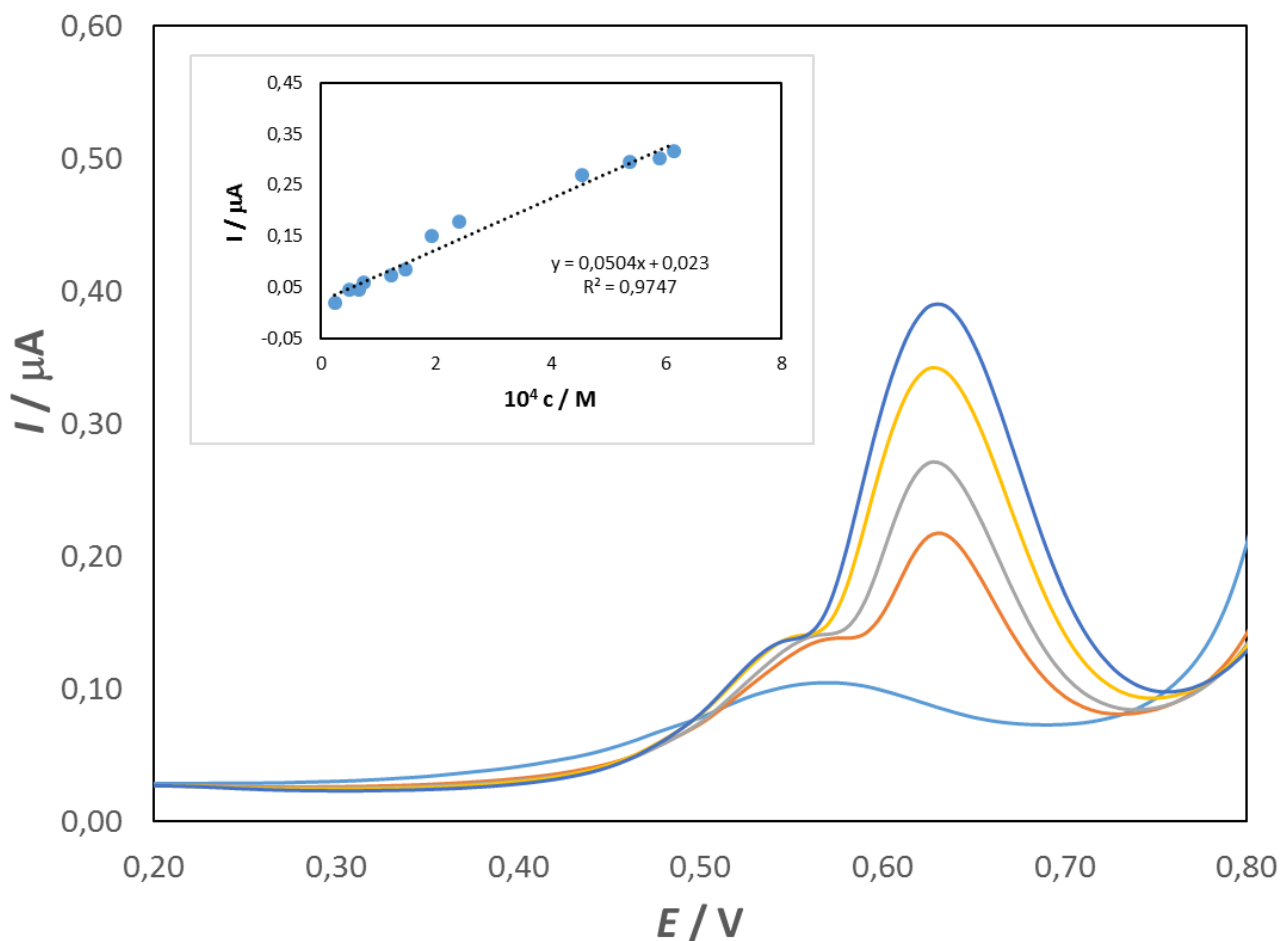


Figure 11. Differential pulse voltammograms in the solutions of compound 1 with concentrations ($c = 6.6 \cdot 10^{-5}$; $1.9 \cdot 10^{-4}$; $2.8 \cdot 10^{-4}$; $4.5 \cdot 10^{-4}$ and $6.1 \cdot 10^{-4} \text{ mol dm}^{-3}$) at a glassy carbon electrode ($I_C = 0.1 \text{ M LiCl}$ in DMF). Scan rate: 5 mV/s .

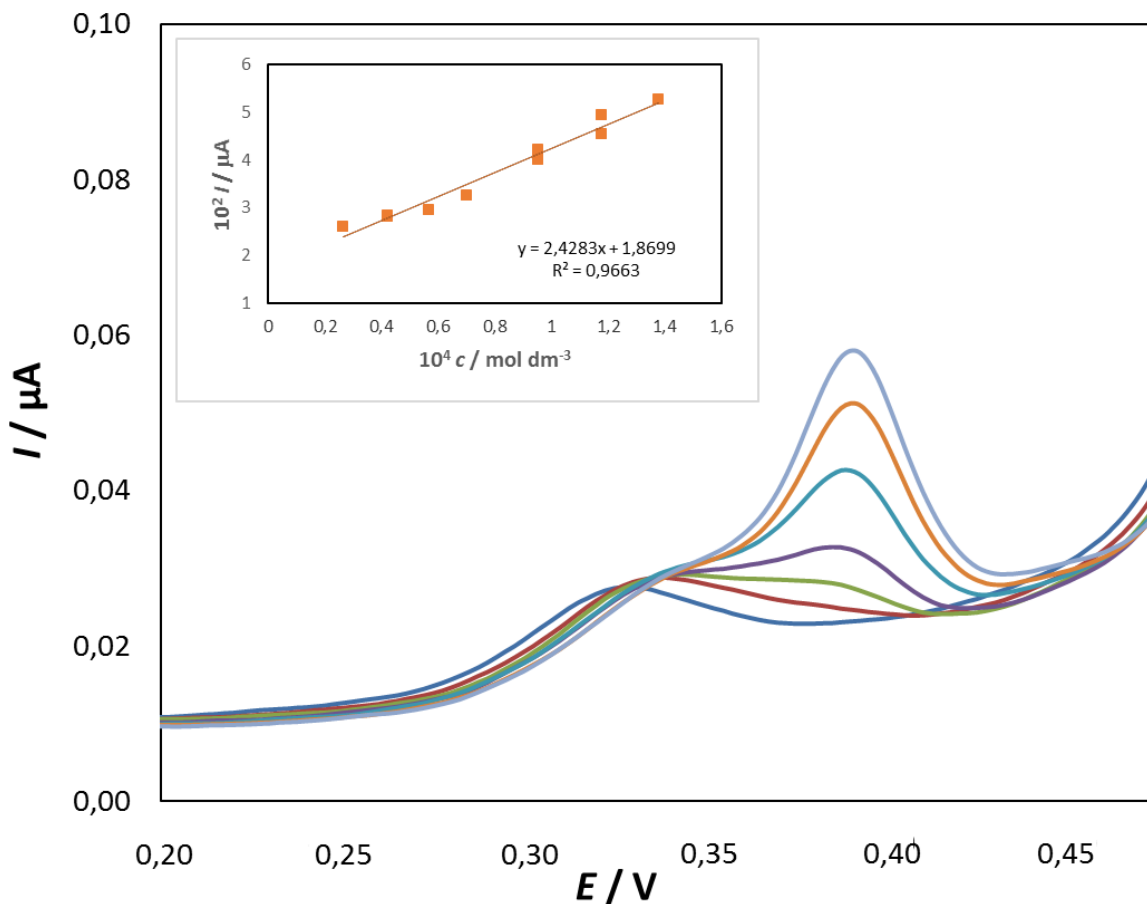


Figure 12. Differential pulse voltammograms in the solutions of compound **2** with concentrations ($c = 0.3 \cdot 10^{-5}$; $0.4 \cdot 10^{-5}$; $0.6 \cdot 10^{-5}$; $0.7 \cdot 10^{-5}$; $1.0 \cdot 10^{-4}$; $1.2 \cdot 10^{-4}$ and $1.4 \cdot 10^{-4}$ mol dm⁻³) at a glassy carbon electrode ($I_c = 0.1$ M LiCl in DMF). Scan rate: 5 mV/s.

4. CONCLUSION

In this study we have synthesized two symmetrical bis-Schiff bases (1E)-1-N-{[4-(4-[(E)-N-(2-aminophenyl) carboxyimido] phenoxy }butoxy)phenyl] methylidene} benzene-1,2-diamine (compound 1) and (1E)-1-N-{[4-(4-[(E)-N-(4-aminophenyl) carboxyimido] phenoxy} butoxy) phenyl]methylidene}benzene-1,4-diamine (compound 2). The compound 1 was characterized by means of single crystal X-ray analysis and both compounds were characterized by spectroscopy (NMR and IR), elemental, TGA/DSC and electrochemical analysis. As it appears, the compound 1 is planar with small deviations of some functional groups and atoms from planarity. The planarity of molecule is supported by strong intramolecular interactions. In the crystal, the molecules are arranged in a herringbone structural motif through the weak N–H \cdots N and C–H \cdots π interactions. The results of IR and NMR analysis along with other structure interpretation methods confirm molecular structure of compound 2. Furthermore, the electrochemical results have shown that the oxidation of the compound 1 is totally irreversible (includes the transfer of one electron) and oxidation of the compound 2 is reversible (follows the EC reaction mechanism) and leads to formation of amine radical which binds to

electrode surface. Oxidation of both compounds is diffusion controlled at the investigated experimental conditions. Adsorption of the oxidation products of both investigated Schiff bases on the glassy carbon electrode occurs and this process is kinetically limited. A linear relationship between peak current and Schiff base concentration in the range of $0.3 \cdot 10^{-4}$ mol dm⁻³ to $6.1 \cdot 10^{-4}$ mol dm⁻³ for compound 1 and in the range of $0.3 \cdot 10^{-4}$ mol dm⁻³ to $1.4 \cdot 10^{-4}$ mol dm⁻³ for compound 2 was established.

ACKNOWLEDGEMENT

The authors thank Josip Juraj Strossmayer University of Osijek, Croatia for financial support.

References

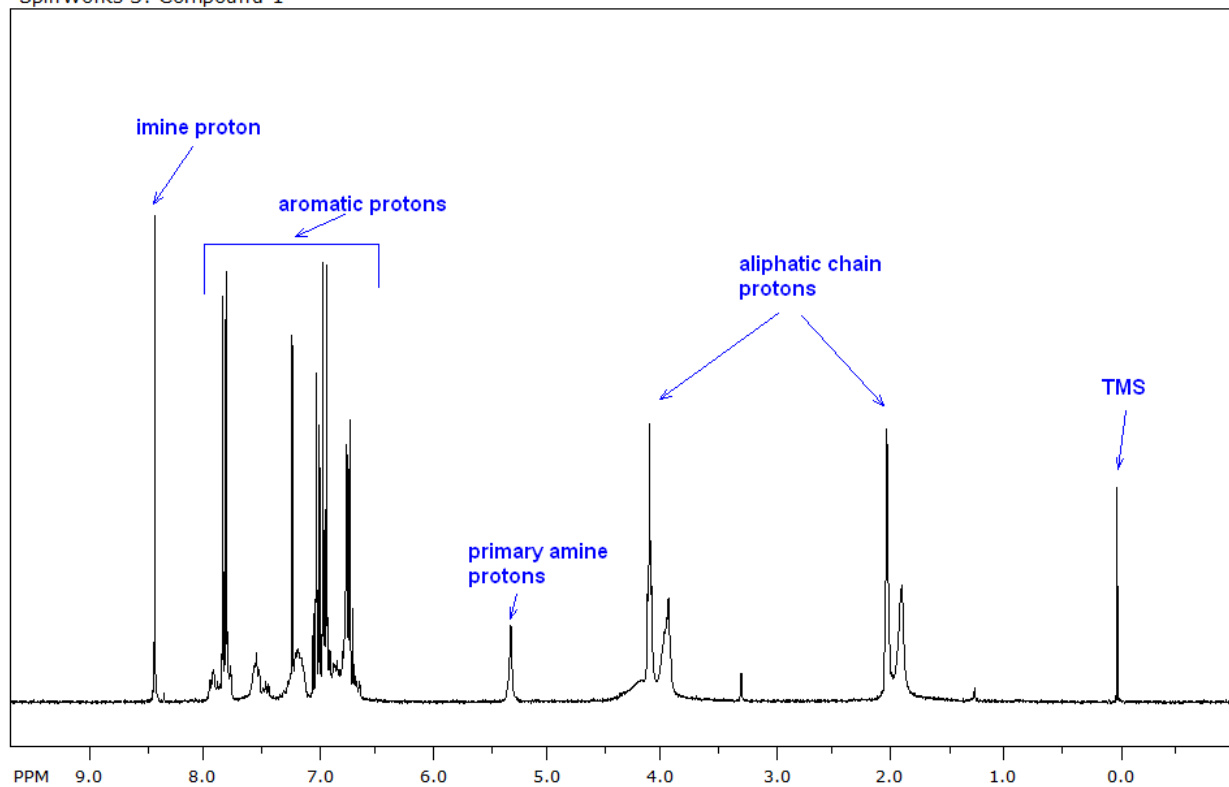
1. A. Iwan, H. Janeczek, B. Jarzabek, P. Rannou, *Materials, Special issue 2* (2009) 38
2. A. Iwan, D. Sek, *Prog. Polym. Sci.*, 33 (2008) 289
3. J. Youn, S. Kewalramani, J. D. Emery, Y. Shi, S. Zhang, H-C. Chang, Y.-j. Liang, C.-M. Yeh, C.-Y. Feng, H. Huang, C. Stern, L.-H. Chen, J.-C. Ho, M.-C. Chen, M. J. Bedzyk, A. Facchetti, T. J. Marks, *Adv. Functional Mat.*, 23 (2013) 3850
4. C. Liang, J. Xia, D. Lei, X. Li, Q. Yao, J. Gao, *Eur J. Med Chem.*, 74 (2014) 742
5. Z. Fang, C. Cao, J. Chen, X. Deng, *J. Mol. Struct.*, 1063 (2014) 307
6. J. Zhao, B. Zhao, J. Liu, W. Xu, Z. Wang, *Spectrochim. Acta A*, 57 (2001) 149
7. V. I. Minkin, A. V. Tsukanov, A. D. Dubonosov, V. A. Bren, *J. Mol. Struct.*, 998 (2011) 179
8. J. E. Anthony, *Chem. Rev.*, 106 (2006) 5028
9. A. H. Kianfar, W. A. K. Mahmood, M. Dinari, M. H. Azarian, F. Z. Khafri, *Spectrochim. Acta A*, 127 (2014) 422
10. G. Grivani, V. Tahmasebi, A. D. Khalaji, *Polyhedron*, 68 (2014) 144
11. B. Shafaatian, A. Soleymannpour, N. K. Oskouei, B. Notash, S. A. Rezvani, *Spectrochim. Acta A*, 128 (2014) 363
12. N. Novoa, F. Justaud, P. Hamon, T. Roisnel, O. Cador, B. Le Guennic, C. Manzur, D. Carrillo, J.-R. Hamon, *Polyhedron*, in press
13. W. Zhang, S. Nu, C. Ma, D. Jiang, *Polyhedron*, 17 (22) (1999) 3835
14. I. N. Booyesen, A. Adebisi, O. Q. Munro, B. Xulu, *Polyhedron*, 73 (2014) 1
15. J. Rohlíček, I. Ketata, T. B. Ayed, R. B. Hassen, *J. Mol. Struct.*, 1051 (2013) 280
16. A. H. Kianfar, S. Ramazani, R. H. Fath, M. Roushani, *Spectrochim. Acta A*, 105 (2013) 374
17. S. Menati, A. Azadbakht, A. Taeb, A. Kakanejadifard, H. R. Khavasi, *Spectrochim. Acta A*, 97 (2012) 1033
18. A. H. Kianfar, M. Paliz, M. Roushani, M. Shamsipur, *Spectrochim. Acta A*, 82 (2011) 44
19. V. Izadkhan, A. Farmany, S. S. Mortazavi, *J. Ind. Eng. Chem.*, in press
20. K. R. Bandi, A. K. Singh, A. Upadhyay, *Electrochim. Acta*, 105 (2013) 654
21. A. A. Abdel Aziz, *J. Lumines.*, 143 (2013) 663
22. K. R. Bandi, A. K. Singh, A. Upadhyay, *Electrochim. Acta*, 105 (2013) 654
23. A. Afkhami, F. Soltani-Felehgari, T. Madrakian, H. Ghaedi, M. Rezaeivala, *Anal. Chim. Acta*, 771 (2013) 21
24. M. Shakir, A. Abbasi, M. Azam, S. N. Khan, *Spectrochim. Acta A*, 78 (2011) 29
25. M. Shakir, A. Abbasi, M. Azam, A. U. Khan, *Spectrochim. Acta A*, 79 (2011) 1866
26. T. Balić, B. Marković, I. Balić, *Acta Cryst. E*, 69 (2013) 126
27. STARE, Software 10.0 (2809), Mettler-Toledo GmbH.
28. Oxford Diffraction (2009) CrysAlis PRO Oxford Diffraction Ltd, Yarnton, England.

29. M. C. Burla, R. Caliandro, M. Camalli, B. Carrozzini, G. L. Casciarano, L. DeCaro, C. Giacovazzo, G. Polidori, R. Spagna, *J. Appl. Cryst.*, 38 (2005) 381
30. L. J. Farrugia, *J. Appl. Crystallogr.*, 32 (1999) 837
31. G. M. Sheldrick, *Acta Cryst. A*, 64 (2008) 112
32. A. L. Spek, *Acta Cryst. A*, 46 (1990) C34
33. A. L. Spek, *PLATON: A Multipurpose Crystallographic Tool*; Utrecht University: Utrecht, The Netherlands (1998)
34. M. N. Burnett, C. K. Johnson, *ORTEP-III: Oak Ridge Thermal Ellipsoid Plot Program for Crystal Structure Illustrations*, Oak Ridge National Laboratory Report ORNL-6895 (1996)
35. F. H. Allen, O. Kennard, D. G. Watson, L. Brammer, A. G. Orpen, R. Taylor, *J. Chem. Soc., Perkin Trans.*, 2 (1987) 1
36. A. Aldenier, M. M. Chehimi, I. Gallardo, J. Pinson, *Langmuir*, 20 (2004) 8243
37. I. Pilac, *Elektroanalitičke metode*, RMC, Zagreb (1995)
38. B. Zeng, S. Wei, F. Xiao, F. Zhao, *Sens. Actuators B*, 115 (2006) 240
39. M. Medvidović-Kosanović, M. Šeruga, L. Jakobek, I. Novak, *Collect. Czech. Chem. C.*, 75 (5) (2010) 547
40. A. Simić, D. Manojlović, D. Šegan, M. Todorović, *Molecules*, 12 (2007) 2327

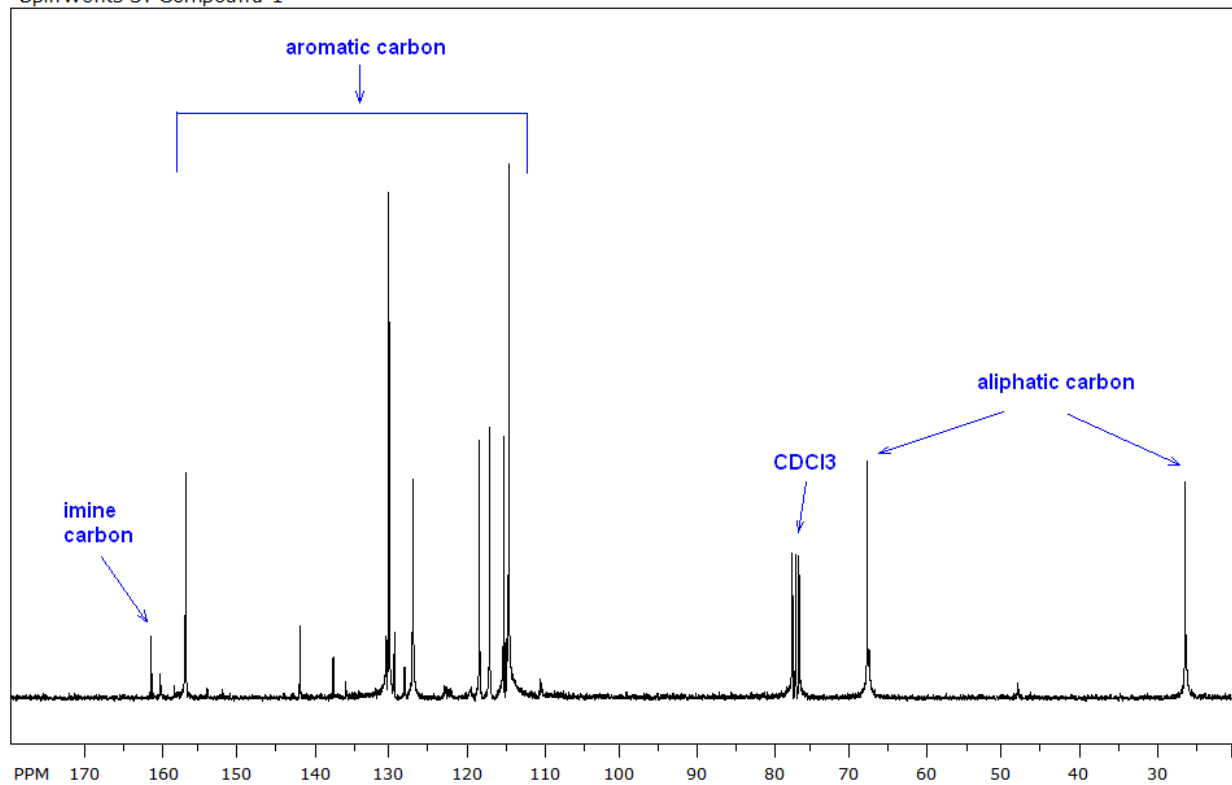
SUPPLEMENTARY DATA:

| S.No | Content | Page No |
|-------------|---|----------------|
| 1 | ¹ H NMR spectrum of the compound 1 | 2 |
| 2 | ¹³ C NMR spectrum of the compound 1 | 3 |
| 3 | ¹³ C NMR spectrum of the compound 2 | 4 |
| 4 | ¹ H NMR spectrum of the compound 2 | 5 |

SpinWorks 3: Compound 1

**Fig. S1.** ^1H NMR spectrum of the compound 1.

SpinWorks 3: Compound 1

**Fig. S2.** ^{13}C NMR spectrum of the compound 1.

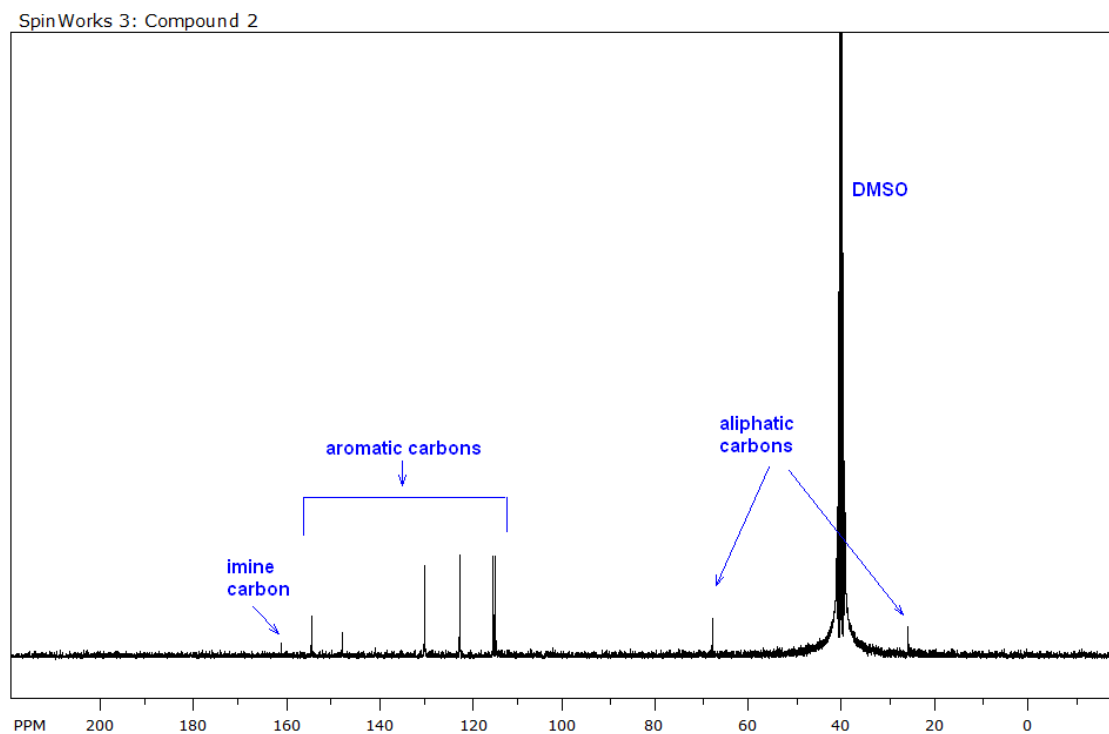


Fig. S3. ^{13}C NMR spectrum of the compound 2.

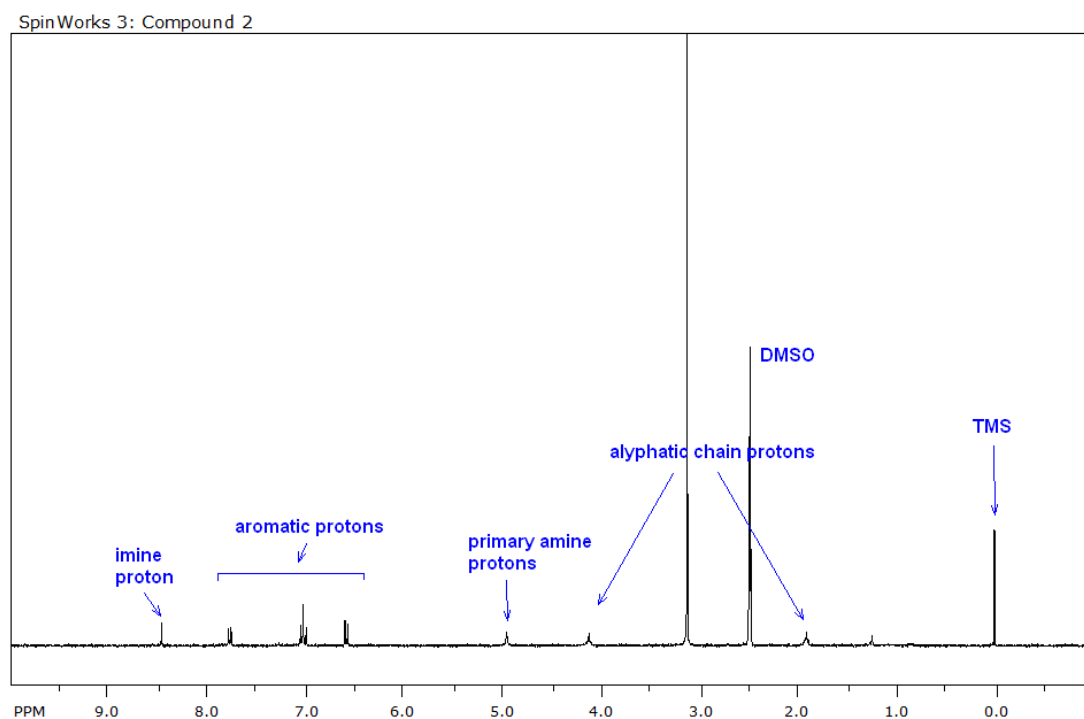


Fig. S4. ^1H NMR spectrum of the compound 2.